Emergence of coherent flow structures over a gravel surface: A numerical experiment

Richard J. Hardy,[1] Stuart N. Lane,[1] Robert I. Ferguson,[1] and Daniel R. Parsons[2]

Received 1 February 2006; revised 21 October 2006; accepted 2 November 2006; published 16 March 2007.

[1] Gravel bed rivers have complex, porous, and irregular surfaces, characterized by a range of morphological forms. These topographical structures determine the flow structures that develop over the river bed, primarily by the shedding of vortices in the downstream wake of protruding clasts. Previous research into these flow structures has come from experimental studies, which have used either flow visualization or single-point measurements techniques. Here we present a numerical experiment where large-eddy simulation (LES) is used to study the generation, evolution, and destruction of these flow structures over a naturally water worked gravel surface. The numerical simulations reported in this paper show that there are two distinct scales of boundary influence upon the shallow flow and emphasize that the measured flow variability at any one point in a natural river will contain both locally derived and upstream-inherited flow structures, according to the range of scales of bed topography present.

Citation: Hardy, R. J., S. N. Lane, R. I. Ferguson, and D. R. Parsons (2007), Emergence of coherent flow structures over a gravel surface: A numerical experiment, *Water Resour. Res.*, *43*, W03422, doi:10.1029/2006WR004936.

1. Introduction

[2] Flow in gravel bed rivers is usually very shallow in relation to the height of the roughness elements forming the bed. The relative submergence (ratio of mean flow depth, d, to typical roughness height, k_s) seldom exceeds 10–20 in flood conditions, and can be less than 5 in normal flows. In such shallow flows the detailed microtopography of the bed exerts a significant effect on the flow [*Wiberg and Smith*, 1991; *Dinehart*, 1992]. An average velocity profile may be approximately logarithmic at $d/k_s \sim 10$, but will have substantial local variation near the bed. These near-bed features relate in the first place to the wakes of individual obstacle clasts, and jets between such clasts, and as such would not be expected to extend much above the tops of the obstacles. Yet, field measurements and laboratory visualization suggest that shallow flows over gravel beds contain coherent macroturbulent structures, often described as consisting of full depth "wedges" of alternately slower- and faster-than-average flow [*Falco*, 1977; *Roy et al.*, 2004]. The origin of these macroturbulent phenomena, and their relationship to the ensemble of individual roughness elements forming the bed, is not well understood.

[3] In this paper we approach this problem in a novel way using large-eddy simulation (LES). Most computational fluid dynamics (CFD) applications to natural gravel bed rivers have represented the channel geometry using boundary fitted coordinates and simulated the time average flow using a turbulence closure scheme to represent the effect of turbulent stresses introduced through Reynolds averaging. Several of the authors of such applications of CFD have commented on the ambiguity of whether the bed microtopography should be represented physically as part of the channel geometry or parametrically through an exaggerated value of the roughness height in a log law representation of flow in the cells adjacent to the bed [*Hodskinson and Ferguson*, 1998; *Sinha et al.*, 1998; *Gessler et al.*, 1999; *Nicholas and Smith*, 1999; *Bradbrook et al.*, 2000; *Booker et al.*, 2001; *Ferguson et al.*, 2003]. Here we take advantage of a recently developed alternative approach to CFD simulation of rivers with irregular beds where detailed bed geometry is represented explicitly through a porosity algorithm approach [*Lane et al.*, 2002; *Lane et al.*, 2004; *Hardy et al.*, 2005]. Because the grid is geometrically rectangular, it is possible to represent the larger scales of turbulence explicitly using LES (see *Keylock et al.* [2005] for a summary of fluvial applications). Here we apply the technique to a shallow flow over a digital elevation model (DEM) based on a natural gravel bed river. The results show that the method works for this natural situation; more importantly, they contain macroturbulent features that resemble those inferred from field measurements and laboratory visualization. The LES results give high spatial resolution in three dimensions through time, in a way that is currently difficult to match by laboratory measurements and impossible to match in the field using currently available technology. The methodology is therefore seen as having considerable potential for elucidating flow structures in shallow streams.

[4] Previous studies of the generation of flow structures in depth-limited boundary flows have principally concentrated on well sorted beds composed of homogenous particles [*Grass*, 1971; *Grass et al.*, 1991; *Krogstad et al.*, 1992]. In these studies, a skimming flow develops, where the momentum exchange mechanism shows strong similarities with bursting processes over smooth surfaces [*Smith*, 1996; *Grass and Mansour-Tehrani*, 1996]. There have been

[1]Department of Geography, University of Durham, Durham, UK.
[2]School of Earth and Environment, University of Leeds, Leeds, UK.

0043-1397/07/2006WR004936$09.00

far fewer studies of turbulence in flows over rough natural gravel surfaces. In this environment, the flow structures which occur in the downstream wake of protruding clasts and/or bed forms, result in the shedding of vortices from the lee of protruding objects [*Robert et al.*, 1993; *Kirkbride*, 1993; *Buffin-Bélanger and Roy*, 1998]. These vortices scale, in the near bed region, with respect to grain size [*Clifford et al.*, 1992; *Clifford and French*, 1993]. As with flow over smooth beds, larger structures may be created by the coalescence and amalgamation of numerous smaller-scale structures [*Head and Bandyopadhyay*, 1981, *Smith et al.*, 1991]. They take the form of high- and low-speed wedges and develop in the outer layer of the flow [*Falco*, 1977; *Kirkbride and Ferguson*, 1995; *Ferguson et al.*, 1996; *Roy et al.*, 2004].

[5] These depth scale (or macroturbulent) eddies are closely linked to the bursting phenomenon in boundary layers [*Grishanin*, 1990; *Yalin*, 1992]. The fluid ejections/sweeps have a quasi-cyclic pattern and are not just restricted to the near bed region, but influence the entire flow field irrespective of bed roughness [*Grass*, 1971; *Talmon et al.*, 1986; *Shen and Lemmin*, 1999]. The ejected low-momentum fluid moves through the entire flow depth up to the water surface, while high-momentum fluid moves from the water surface toward the bed [*Grass et al.*, 1991]. This gives rise to rolling structures [e.g., *Klaven*, 1966; *Klaven and Kopaliani*, 1973; *Imamoto and Ishigaki*, 1986a, 1986b]. There is a general consensus as to the pattern of the bursting phenomenon in the near bed region [*Nezu and Nakagawa*, 1993]. However, opinion differs about the ordered depth scale motions in open channel flows [*Shvidchenko and Pender*, 2001]. Observations have reported streamwise spacing length scales of between 2 and 7 times the water depth (d) for these bursting events [*Sumer and Deigaard*, 1981; *Nezu and Nakagawa*, 1993; *Best*, 1993; *Nikora and Goring*, 1999; *Sechet and Le Guennec*, 1999; *Shvidchenko and Pender*, 2001]. Furthermore, *Yalin* [1992] argues that the depth scale eddies are neither permanent nor do they originate in their full size (d), but are generated near the bed as a result of a burst and then grow until the size becomes nearly equal to d. They are then destroyed, promoting a generation of new eddies and causing a cycle of positive feedback. The complete cycle occurs over a distance of 6 d [*Shvidchenko and Pender*, 2001], although the definition of d over these complex surfaces is difficult. It also remains unclear as to why high- and low-speed regions exist alternately in the streamwise and spanwise direction in turbulent flow [*Nychas et al.*, 1973; *Falco*, 1977; *Kirkbride and Ferguson*, 1995; *Ferguson et al.*, 1996; *Buffin-Belanger et al.*, 2000; *Roy and Buffin-Belanger*, 2000]. Some authors have explained this in terms of the bursting phenomenon [*Yalin*, 1992; *Nezu and Nakagawa*, 1993]. Others have explained the sequence of high- and low-speed regions by the downstream motion of large-scale turbulent eddies [*Shvidchenko and Pender*, 2001].

[6] Given the above, it is clear that a full understanding of the cause and regularity of macroturbulent fluctuation in shallow flows over gravel beds does not exist. Process information derived from data collected from laboratory experiments and field studies provides contradictory evidence. Some studies have been interpreted as showing low-frequency velocity fluctuations corresponding to a spatial scale of the order of the flow depth [*Komori et al.*, 1982; *Grinvald and Nikora*, 1988; *Clifford et al.*, 1992; *Lapointe*, 1992; *Nezu and Nakagawa*, 1993; *Robert et al.*, 1993; *Roy et al.*, 1996; *Cellino and Graf*, 1999; *Shen and Lemmin*, 1999]. Other authors do not detect any regular period in turbulent fluctuations [*Grinvald*, 1974; *Nikora and Smart*, 1997], which suggests coherent structures are randomly distributed in time and space [*Nychas et al.*, 1973; *Smith*, 1996; *Nikora and Goring*, 1999]. Studies of turbulent structures in gravel bed rivers in the field are limited because of the challenges of instrumentation [*Roy et al.*, 1996]. This has considerable significance if a high-resolution (individual particle) understanding of sediment transport is to be developed in such an environment as a complete understanding of the driving forces is required.

2. Methodology

2.1. Numerical Simulation of Flow Over Complex Microtopography

[7] The incorporation of complex microtopographies (individual particles) within a CFD scheme has been problematic to date as the representation of large-scale topographic features has required the application of boundary fitted coordinates (BFCs), which involve mesh deformation in the Cartesian space (though not in the computational space). Mesh deformation may increase the numerical diffusion in a CFD model application and lead to uncertainties as to whether observed changes in process representation are due to topographic effects or grid adjustment effects. Moreover, the mesh distortion increases as the resolution of spatial discretization increases as the topographic information becomes more complex. Second, the subgrid-scale topography (e.g., grain surface morphology, grain interactions) within the CFD scheme has traditionally been represented using a roughness parameter which represents the frictional retardation of the flow in the cell touching the bed. Most commonly, the representation of topographic variability involves specification of a friction height (z_o) in some sort of wall function and the multiplication upward of the equivalent sand grain roughness. In a 3-D modeling framework, this assumes that the topographic variability that is not included in the model geometry is represented as a subgrid-scale effect through this upscaling. There is debate over which grain parameter to upscale and by how much. For instance, field investigations suggest that z_o should, including upscaling, take a value of about 0.1 D_{84} [*Whiting and Dietrich*, 1990; *Wiberg and Smith*, 1991] or when specified as k_s, (where $k_s = 30\ z_o$) 3.5 D_{84} or 6.8 D_{50} [*Hey*, 1979; *Bray*, 1982], which has been derived from either fitting the log law to a single velocity profile or from cross-sectional average mean velocities. These estimates of roughness height may be problematic for 3-D CFD applications where the wall function is only applied to the boundary cells, not full (or even part) of the flow profile. Furthermore, it has been shown that the multiplication of roughness length represents a measure of total flow resistance that incorporates contributions from both individual grains and larger bed forms [*Wiberg and Smith*, 1991; *Clifford et al.*, 1992].

[8] These uncertainties aside, the wall function approach is associated with a number of problems in 3-D CFD

applications. These include (1) the multiplier of roughness length will need to be spatially variable and scale dependent, in relation to both mesh resolution and the topographic content of the data set used to describe the surface, (2) reduced numerical stability and solution accuracy for flows characterized by high relative roughness [e.g., *Nicholas and Smith*, 1999] because of the existence of an upper limit of k_s for a given near-bed cell thickness [*Nicholas*, 2001], and (3) the basic problem of setting the reference height of the bed in a numerical mesh: normally, it is assumed implicitly that the effective bed surface in mass conservation terms is the same as the bed surface sampled during field survey.

[9] An alternative approach has recently been developed for incorporating complex river bed topographies into regular structured meshes, without the need to use boundary fitted coordinates [*Lane et al.*, 2002, 2004; *Hardy et al.*, 2005]. It uses a porosity method based upon the work of *Olsen and Stokseth* [1995] and involves the use of a regular structured grid in which all control volumes are orthogonal in both computational and Cartesian space, with the bed topography specified using cell porosities (P). This approach has been successfully validated using digital particle image velocimetry (DPIV) as applied to an irregular arrangement of cuboidal roughness elements [*Hardy et al.*, 2005] and for the case of time-averaged flow over rough gravel beds [*Lane et al.*, 2004]. The development of this method has allowed an understanding of the way in which a complex gravel bed surface interacts with the associated flow field and provides the opportunity for understanding the interaction between gravel bed topography and the associated 3-D flow field.

2.2. Large-Eddy Simulation

[10] In this paper, we couple the porosity bed form representation method to large-eddy simulation (LES) in order to study time-dependent flow structures over a gravel surface. Modeling flows over complex topography is problematic [*Patel*, 1998] and only recently have attempts been made to model such flows using LES [*Ciofalo and Collins*, 1992; *Lee*, 2002]. Recent applications of LES to fluvial problems include flow at a parallel channel confluence [*Bradbrook et al.*, 2000]; flow and sediment transport over both two and three dimensional bed ripples [*Zedler and Street*, 2001]; and flow over surface-mounted transverse ribs [*Cui et al.*, 2003].

[11] LES calculates the properties of all eddies larger than the filter size and models those smaller than this scale by a subgrid-scale (SGS) turbulence transport model [*Gullbrand and Chow*, 2003]. There are several theoretical summaries of the principles of LES [*Lesieur and Métais*, 1996; *Lesieur et al.*, 1997; *Rodi et al.*, 1997; *Sagaut*, 1998; *Meneveau and Katz*, 2000; *Piomelli and Balaras*, 2000; *Fröhlich and Rodi*, 2002; *Moin*, 2002; *Keylock et al.*, 2005]. Central to LES is one core principle: the grid size that is resolved is sufficient to represent the scales of time-dependent features present in the flow. This means that mesh design issues are crucial. The porosity algorithm described above is important: it maintains a constant mesh size in space and so allows simulation of time-dependent flow structures using LES.

[12] There are two important factors which need consideration in the construction of a LES scheme: (1) the choice of filter and (2) the subgrid-scale model (SGS). In LES a length scale is required to determine a filter size. This is often taken to be equal to the grid size employed in the solution of the equations: then eddies larger than the filter scale are solved directly; and the effects of eddies less than the filter scale are modeled using a subgrid-scale treatment. A series of appropriate filters were initially defined by *Leonard* [1974]. Since then, the box (top hat) filter has been the most common choice [*Deardorff*, 1970a; *Clark et al.*, 1979; *Silveira Neto et al.*, 1991], although Gaussian filters [*Vreman et al.*, 1994] and spectral cutoff filters [*Härtel and Kleiser*, 1998] have also been used. It has been suggested that the choice of filter makes little difference to the solution [*Härtel*, 1996; *Härtel and Kleiser*, 1997] and the choice of the SGS is more important.

[13] SGS models represent the exchange of energy between the grid and subgrid scales. In turbulent flows energy transfer is typically from the larger to the smaller eddies (energy cascade) although this process may not be continuous especially where eddies impinge upon either a solid surface or in shear layers. Here an inverse transfer of energy between scales is possible and is important for the growth of turbulence in wall-bounded flows [*Piomelli et al.*, 1990]. Therefore an ideal SGS model should be able to capture both the forward and inverse energy transfers. This has proven to be a major stumbling block for the development of SGS models. Indeed, there are several SGS models that can be applied and a considerable amount of literature on the problem.

[14] The original SGS model, from which most schemes have evolved, is the Smagorinsky SGS model [*Smagorinsky*, 1963]. This is an eddy viscosity model which is absolutely dissipative: it only accounts for energy transfer from large to small eddies. This model was initially adopted by *Deardorff* [1970a, 1970b] to study turbulent channel flow and the planetary boundary layer. It has proved to be particularly popular in a range of literatures [*Bedford and Babajimopoulos*, 1980; *Moin and Kim*, 1982; *Cai and Steyn*, 1996] although the scheme has been criticized as being over reliant on the Smagorinsky constant, C_s. The value for C_s has been obtained theoretically from the Kolmogorov constant C_k; the constant in the Kolmogorov energy cascade of turbulence from large to small scales. Constant values range from 0.17 [*Schumann*, 1991] to 0.1 for turbulent channel flow [*Deardorff*, 1970a; *Moin and Kim*, 1982] and have been shown to be both a function of time and space that varies between 0.07 and 0.24 [*Rogallo and Moin*, 1984]. Thus C_s varies with the type of flow as different processes contribute to the value of C_s [*Canuto and Cheng*, 1997]. With these limitations in mind, several alternate SGS models have been proposed.

[15] One of the simpler alternatives is the scale similarity model [e.g., *Bardina et al.*, 1980] which is based on the assumption that the most important unresolved eddies are those of a size just smaller than the filter size. Here a double filter is implemented which has the advantage that it is potentially possible for backscatter effects to be mimicked at the subgrid scales. However, the scale similarity model does not dissipate sufficient energy and is therefore often employed in combination with the Smagorinsky model. It is also possible to define a spectral eddy viscosity [e.g., *Chollet and Lesieur*, 1981] (see *Lesieur et al.* [1999] for a

complete review]) where the effective eddy viscosity is obtained as a function of the cutoff wave number by assuming a spectrum with a slope of $-5/3$ and a cutoff at the boundary between the resolved and unresolved scales.

[16] Another development in SGS modeling has been dynamic methods, where a second "test" filter is employed to evaluate C_s as a function of both time and space [*Germano et al.*, 1991; *Germano*, 1992; *Meneveau and Katz*, 1999]. This approach uses the smallest scales of the resolved turbulence to provide information about the local value for the SGS model coefficient through a dynamic Smagorinsky coefficient (C_d). The Germano approach relates the resolved turbulent stresses to the subgrid and subtest-scale stresses where the coefficient is moved outside of the filtering operation and locally chosen, thus minimizing the residual error. Since the original methodology there have been several modifications. One of the most significant was that of *Lilly* [1992] who introduced a least squares technique to evaluate C_d to give a local dynamic model. However, there are some important theoretical and practical difficulties with the original dynamic model formulation. These have been addressed with the development of enhanced dynamic SGS modeling. By moving the coefficient outside of the filter, the relation between neighboring values for the coefficient is eliminated. This leads to too much variability in the coefficient field, including the production of negative eddy viscosities. Potentially this allows the possibility of representing an inverse energy transfer, but it tends to destabilize the numerical solution as regions of negative viscosity persist and grow. It is possible to deal with this by "clipping" negative values to positive [*Zang et al.*, 1993] and/or assuming at least one homogeneous direction in the flow and averaging the coefficient over this direction to generate a more smoothly varying field for C_d [*Moin et al.*, 1991].

[17] Another method of incorporating the inverse energy cascade is to add a stochastic term into the SGS modeling [*Mason and Thomson*, 1992]. However, if the backscatter is modeled as noise which is not temporally autocorrelated, there is an implicit scale separation between the smallest resolved eddies and the eddies just smaller than the filter size [*Ghosal et al.*, 1995]. Stochastic representation of the inverse cascade within the framework of dynamic localization has been developed by introducing an eddy force at both the grid and test filter scale, which was modeled as a zero-centered white noise process [*Carati et al.*, 1995]. To prevent the global minimization becoming a stochastic problem, the errors resulting from using modeled as opposed to known values for C_s were averaged over the possible realizations of the noise for a particular velocity field. This removed any effect due to mean behavior, but retained an effect upon the flow energy. However, these approaches are computationally demanding.

[18] In order to reduce computational demands, several developments have occurred. These include an approximation to the integral required in the dynamic localization method based on time extrapolation [*Piomelli and Liu*, 1995] as well as ensemble averaging to determine the effect of small scales on the modeled flow [*Meneveau et al.*, 1996]. This approach defines the temporal averaging: A timescale based on the smallest resolved eddies calculated from a Lagrangian trajectory of fluid packets. The defined averaging is sufficiently flexible to allow a shorter time frame for averaging in regions of high strain and to permit less weight to be attached to values representing backscatter. Furthermore, the simulation of eddy structures showed that the use of Lagrangian averaging reduced the dissipation for ejection events, giving more realistic results than standard averaging [*Meneveau et al.*, 1996]. Moreover, a scale-dependent dynamic subgrid-scale model has been developed which unlike the traditional dynamic model does not rely on the assumption that the model coefficient is scale invariant [*Porté-Agel et al.*, 2000]. This approach is based on introducing a secondary test filter that, in addition to the traditional test filter, is used to determine both the coefficient and how it changes across scales [*Porté-Agel et al.*, 2000]. Validation experiments of the new model, looking at velocity spectra from simulations of an atmospheric boundary layer, show that the model improves the predictions of spectral slopes at different heights from the ground as in the near-surface region, the traditional Smagorinsky model is too dissipative and traditional dynamic models are not dissipative enough [*Porté-Agel et al.*, 2000].

[19] Finally, another approach for subgrid-scale models has been to optimize the scales that are available in the LES. This has been called both "inverse modeling" [*Geurts*, 1997] and "approximate deconvolution" [*Domaradzki and Saiki*, 1997; *Domaradzki and Loh*, 1999; *Stolz and Adams*, 1999; *Stolz et al.*, 2001]. *Hughes et al.* [1998, 2001a, 2001b] and *Collis* [2001] have demonstrated a variational multiscale method where better LES results are obtained if the solved equations are split into small- and large-scale representations and only the shear stresses extracted at the smaller and unresolved scales are modeled.

[20] The above review demonstrates the range of developments in LES from the original Smagorinsky model. It is acknowledged that the original Smagorinsky model has limitations and considerable improvements have been made, especially in terms of dynamic modeling procedures. This paper is the first that uses a LES approach to study flow over and around individual gravel particles to gain insight into process representation at the river bed. Thus we begin with an application of a standard Smagorinsky model within the porosity algorithm framework to see if the approach produces physically realistic results, and prior to the application of a more complex formulation.

2.3. Experimental Design: Laboratory Data Collection

[21] The experimental setup used for model development was the same as used by *Lane et al.* [2004]. It is based upon water worked gravels in a 0.30 m wide and 8.0 m long tilting flume. A bulk sample of sediment from the River Affric, Scotland was placed in the flume (D_{50} = 0.020 m; D_{84} = 0.069 m, max length scale 0.056 m) and water worked until a stable bed (no sediment transport) with a realistic structure was obtained. Once the gravels had been water worked, the surface morphology was measured using two media digital photogrammetry (see *Butler et al.* [2002] for full explanation). The experimental setup allowed generation of DEMs at a spacing of 0.001 m. These DEMs have been subject to intensive data quality tests, in terms of point precision and accuracy and surface precision and accuracy [e.g., *Butler et al.*, 1998, 2001, 2002]. The topography (Figure 1) had a mean surface error of 0.0008 m and the standard deviation of error was ±0.0017 m.

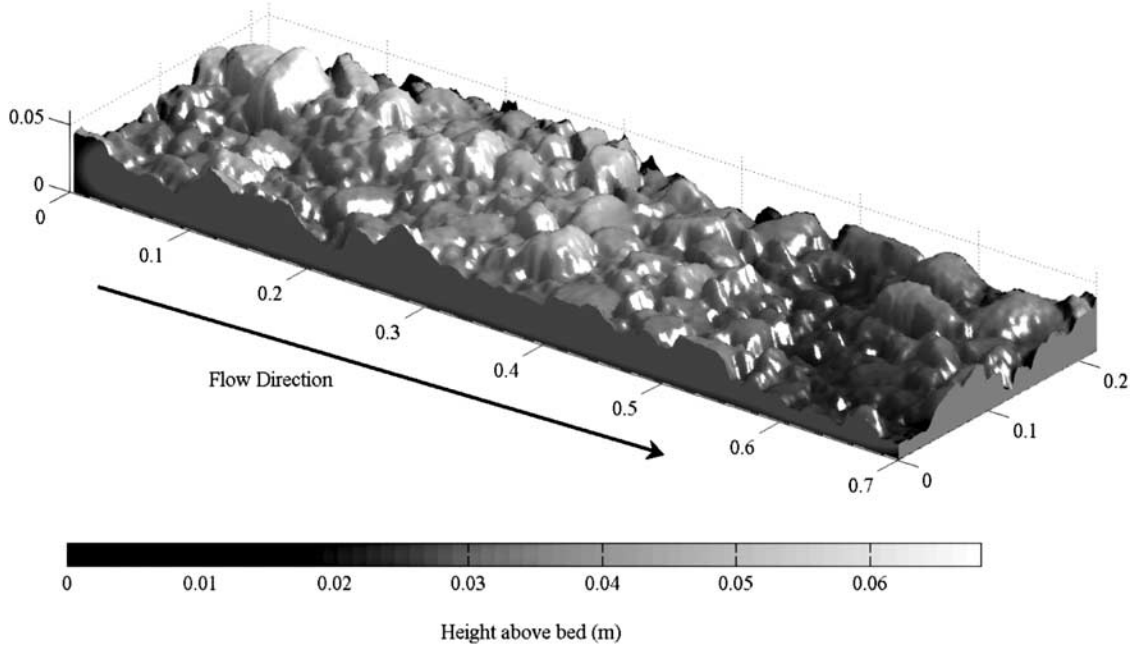

Figure 1. Digital elevation model of the flume bed used in this study. The scale represents the topographic height in the DEM.

2.4. Application of Numerical Model

[22] We used a 0.70 m long and 0.20 m wide section of river bed gravels to define the bed geometry. The computational domain was regular in the x (downstream), y (cross stream) and z (vertical) directions, with a grid resolution of 0.002 m. In the vertical, to allow inclusion of topography data using the porosity treatment, the maximum extent of the domain was set at 0.06 m. Thus the computational grid comprised $350 \times 110 \times 30 = 115\,500$ cells. With a depth average inlet velocity of 0.24 m s^{-1} the flow has a Reynolds number of approximately 11 000 and a Froude number of 0.31. This is a very shallow flow ($d/D_{50} \approx 3$, $d/D_{84} \approx 1$) corresponding to a low discharge in the prototype river. A RANS simulation of flow over this surface has been validated for a flume experiment with a mean flow depth of 0.24 m against velocity profiles collected with a NorTek acoustic Doppler velocimeter (ADV) measuring at 0.010 m intervals above the bed at the planform locations [*Lane et al.*, 2004]. We needed to reduce the flow depth to a maximum 0.06 m for computational reasons in this study, which precluded validation of the scheme used. Further, *Lane et al.* [2004] also show that the ADV measuring volume is too coarse in relation to model resolution: it commonly contains $5 \times 4 \times 4$ grid cells which means that it does not resolve local flow gradients fully. Instead, we undertake a higher level validation (see below) by exploring how model predictions compare with our general understanding of shallow flows over gravel beds obtained from flume and field studies.

[23] In this study, we began by obtaining a steady state solution using a RNG two-equation k-ε turbulence model as the initial condition for an unsteady simulation with the LES model. In this application the full non linear, filtered Navier Stokes equations are solved. Here, a cutoff point is defined in the spectrum of turbulent scales based on the grid dimensions, in this case 0.002 m. Eddies capable of being resolved by the computational grid are allowed to evolve according to the Navier-Stokes equations and a turbulence model [*Smagorinsky*, 1963] is only employed to represent the effects of turbulence at subgrid scales (SGS). The Navier-Stokes equations are averaged over the cell volume [*Schumann*, 1975] and, as with Reynolds averaging, produce unknown stresses related to SGS motion. These stresses (τ_{ij}) are given by

$$\tau_{ij} = -2\rho\nu_t S_{ij} \tag{1}$$

where ρ is the fluid density, ν_t is the eddy viscosity and S_{ij} is the local mean strain rate:

$$S_{ij} = 0.5\left(\frac{\partial u_i}{\partial x_j} + \frac{\partial u_j}{\partial x_i}\right) \tag{2}$$

where u_i is the component of velocity in the direction x_i. The eddy viscosity is determined using a mixing length relationship:

$$\nu_t = l^2\left(2S_{ij}\frac{\partial u_i}{\partial x_j}\right)^{\frac{1}{2}} \tag{3}$$

The mixing length, l, is the characteristic length of unresolved eddies, defined as

$$l = \min(C_s h, \kappa . d_{wall}) \tag{4}$$

where C_s is the Smagorinsky constant, κ is the von Karman constant (taken as 0.4), d_{wall} is the normal distance to the nearest wall, and h is the representative mesh interval:

$$h = \sqrt{\frac{dx^2 + dy^2 + dz^2}{3}} \tag{5}$$

which simplifies to

$$h = \sqrt{dx^2} \text{ as } dx^2 \equiv dy^2 \equiv dz^2 \quad (6)$$

where dx, dy, dz are the local mesh dimensions in the three coordinate directions. This eddy viscosity model is isotropic and implicitly assumes the SGS turbulence is in equilibrium with the large eddies at the scale at which it is applied and adjusts itself instantaneously to changes of the large-scale velocity gradients.

2.5. Boundary Conditions

[24] Boundary conditions needed to be specified at the upstream inlet, downstream outlet, sidewalls and free surface. For the steady state solution the upstream inlet is calculated from the experimentally acquired ADV data and the downstream outlet is specified as a fully developed flow profile with the hydrostatic pressure set at the surface at the downstream outlet. For the LES simulation cyclic boundary conditions were applied, implying that the domain is infinitely long. At the sidewall, no-slip conditions were applied. At the free surface, we use a method applied by *Bradbrook et al.* [2000]. This uses a symmetry plane at the surface across which all normal resolutes are set to zero. To represent the effects of water surface variation, nonzero pressure terms on the symmetry plane are introduced to the momentum equations, commonly referred to as a rigid lid treatment. This allows for the effects of both water surface superelevation and depression with respect to the plane in terms of the momentum equations. However, if the mass conservation equations are not corrected, it will lead to under estimation of velocities in zones of water surface depression and over estimation of velocities in zones of water surface superelevation. To deal with this, we introduce an effective surface cell thickness (ΔZ_{sij}) into the continuity equation, which scales the equivalent cell face area in the cross-stream and downstream directions according to the pressure (P_{sij}) on the symmetry plane at cell (i, j)

$$\Delta Z_{sij} = \left(\frac{P_{sij} - \rho g h_{cij}}{\rho g h_{cij}}\right) + \Delta Z_{ij} \quad (7)$$

where h_{cij} is the elevation of the surface grid cell at location (i, j). *Bradbrook et al.* [2000] show that this yields a stable approximation of free surface elevation provided spatial gradients of water surface are not too great, and normally not greater than ΔZ_{ij}. This is evaluated with each application of the model.

[25] A finite volume method is used to discretize the equations, and in this case a Cartesian mesh is applied. The interpolation scheme used is hybrid upwind where upwind differences are used in high convection areas (Peclet number > 2) and central differences where diffusion dominates (Peclet number < 2). Use of the Peclet number guarantees that in situations where diffusion dominates, a higher-order solution is used which reduces the tendency for numerical diffusion. This method is also stable and as the aim is to investigate periodic aspects of the flow, this approach is important in order to avoid the introduction of spurious oscillations in the solution which can occur with some higher-order numerical schemes. Coupling of the pressure and momentum equations is achieved using SIMPLEST, a variation on the SIMPLE algorithm of *Pantankar and Spalding* [1972].

3. Results

[26] We interpret model output in four stages. Initially, visual analyses of the numerical results are presented. This is followed by analyzing the results in terms of correlation in the downstream (u') and vertical (w') velocity deviations in order to match classical approaches to interpreting field and flume data. Next, the results are analyzed in terms of quadrant analysis. Quadrant analysis has previously been used to discriminate boundary layer turbulent events by examining the instantaneous deviations of velocity from the mean values [e.g., *Lu and Willmarth*, 1973; *Bogard and Tiederman*, 1986; *Bennett and Best*, 1995]. For this reason, it is the focus of the analysis in this paper. Applying the standard definition of *Lu and Willmarth* [1973], four quadrants can be defined around a zero mean: (1) quadrant 1 describes outward interactions (positive u component, positive w component), (2) quadrant 2 describes ejections (negative u component, positive w component), (3) quadrant 3 describes inward interactions (negative u component, negative w component, and (4) quadrant 4 describing inrush events (positive u component, negative w component. In a turbulent boundary layer, quadrant two (ejection) and quadrant four (sweep) events are dominant. Finally the energy spectra for the downstream velocity component are calculated at 0.2 and 0.8 z/h for two profiles located at 0.21 and 0.61 x/l. The limitation of the Smagorinsky SGS model is that it is too dissipative [*Mason and Thomson*, 1992]. The dissipation characteristics of the model have a direct impact on the turbulent kinetic energy of the resolved velocity field, which in turn affects the shape of the mean velocity profile [*Porté-Agel et al.*, 2000]. In order to assess the model's performance the energy spectra are calculated to assess the decay at high wave numbers.

3.1. Flow Visualization

[27] Figure 2 shows a series of velocity magnitude (the resolved components of u, v, and w) plots in plan view (x y slices), 0.036 m from the bed. Each image is spaced 1 second apart. The images show a strongly streaky pattern, with areas of fast flow around large particles (A in Figure 2a) and wakes in the lee of such particles (e.g., B in Figure 2a). In region A (Figure 2a) a region of high flow velocity arising from flow separation around a large protruding particle can be observed. This appears to be quasi stationary, its core being present in all of the images covering the 10 s period. The structure of this feature has similar characteristics to the horseshoe vortex observed in classic fluid mechanics. In region B there is a relatively stable region comprising a low-momentum recirculation cell (i.e., a wake) with possibly an arch vortex similar to that identified by *Hunt et al.* [1978]. Typically these features would have been predicted by the application of a RANS turbulence closure model [e.g., *Lane et al.*, 2004], although time averaged turbulence models (e.g., the two equation k-ε model) are poor at predicting separation lengths [*Hardy et al.*, 2005]. However, region C marked on Figure 2b comprises a region of flapping, downstream from the object. This region is downstream of the high topography (Figure 3) and in a zone of deeper flow. Here time-dependent flow structures evolve

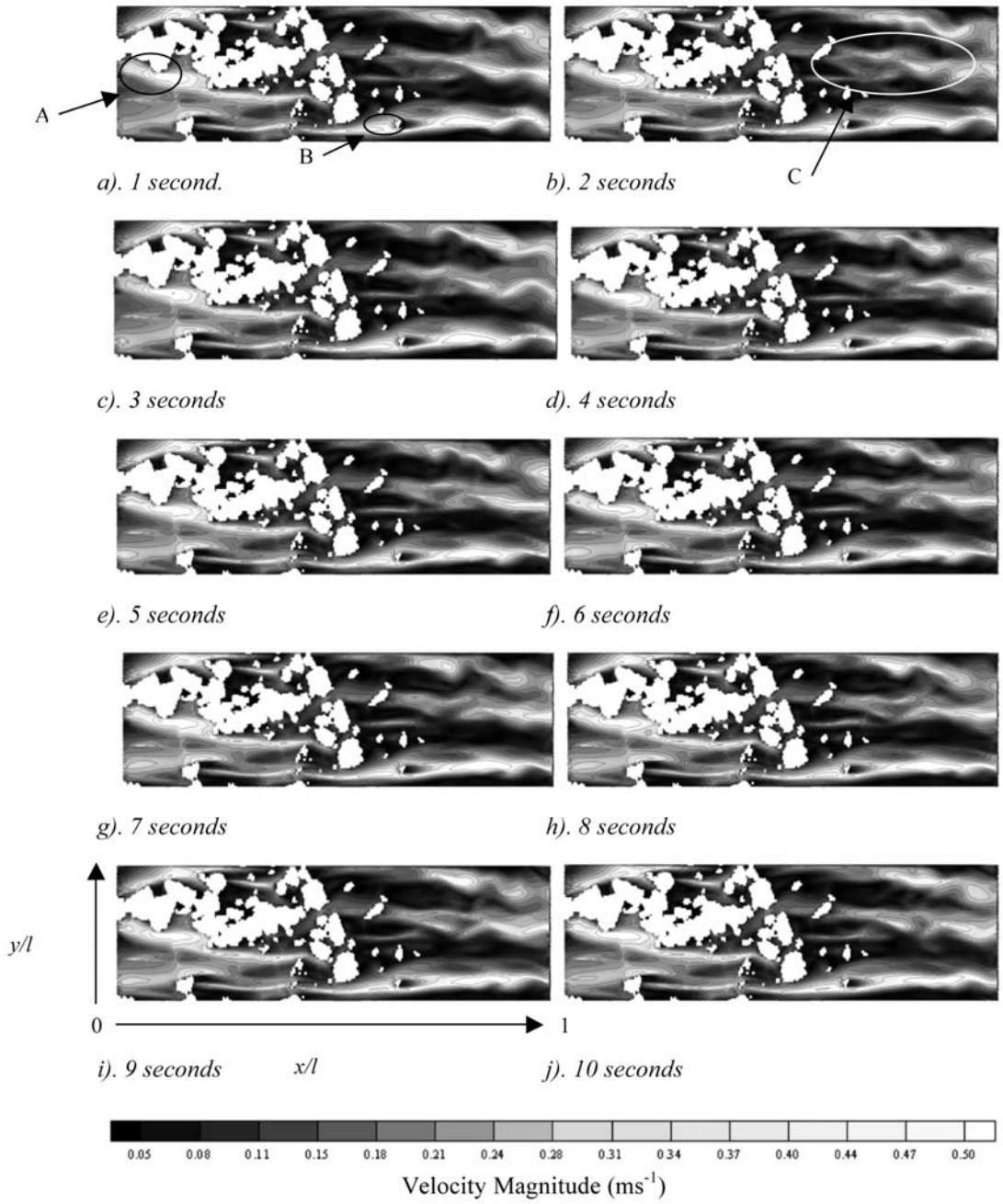

Figure 2. Plan view of the velocity magnitude at a horizontal slice 0.036 cm above the bed through time. The white regions are zones of pebbles blocked out of the numerical domain by the porosity algorithm. Figure 2a is 100 s into the simulation.

and complex flapping of structures can be easily observed. This is considered further in terms of time series analysis below.

[28] Figure 3 shows a series of w (vertical) component velocity plots for the centre line. In Figures 3a–3d, upward flow can be observed as the flow interacts with the first large clast (x/l = 0.27) and shows similarities to classical junction vortex flow. Downstream from this object, the flow is periodic. For example, in the deepening section of the flow (x/l = 0.8) oscillation between upward and downward flow can be observed. This oscillation extends throughout the flow depth and, as such, appears to be very similar to the fluid wedges which have previously been observed in gravel bed rivers. In qualitative terms, these results are encouraging.

3.2. Time Series of Fluctuating Velocities

[29] Figure 4 shows example time series of the vertical component for a 5 s period for a zone of flow shallowing (i.e., the stoss of a particle, Figures 4a and 4b) and a zone of flow deepening (i.e., as in the lee of a particle, Figures 4c and 4d). These plots show clear quasiperiodicity in the

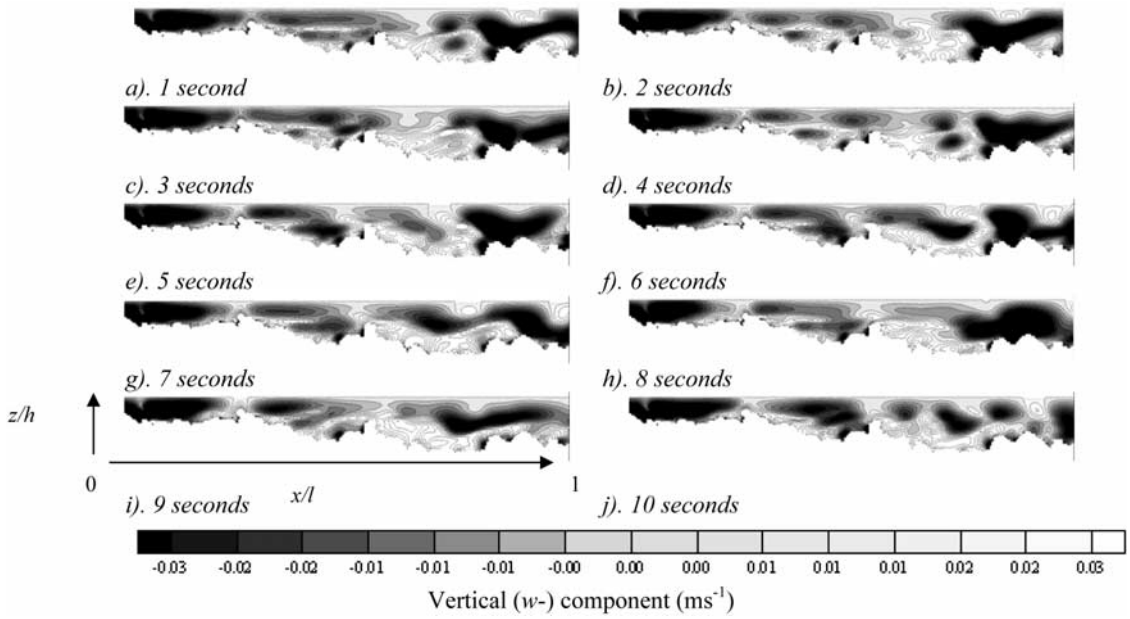

Figure 3. Vertical slice of the vertical velocity component down the midline. The white regions are zones of pebbles blocked out of the numerical domain by the porosity algorithm. Figure 3a is 200 s into the simulation.

turbulence signal. From $x/l = 0.21$ to $x/l = 0.27$, the flow shallows, and the result is a reduction in the magnitude of vertical velocity fluctuations at all heights within the flow, coupled to slight stretching of the wavelengths. At $x/l = 0.21$ (Figure 4a), flow which is closer to the surface ($z/h = 0.8$) leads flows at the bed. By $x/l = 0.27$, this lead is diminished, and the fluctuations are more synchronous as well as being of smaller magnitude. This probably reflects the growing influence of the bed as the flow shallows, with resistance having a greater effect closer to the bed, and fluctuations in velocity from upstream traveling more slowly at the bed. As the bed shallows, the effects of resistance are more strongly felt throughout the flow, and the fluctuations are more synchronous, and reduced in magnitude. As the flow deepens (Figures 4c and 4d), the fluctuations are more variable in terms of magnitude and timescale and, as a result, appear to be less organized.

[30] The level of organization is greater as the flow starts to deepen ($x/l = 0.50$, Figure 4c) than when it becomes deeper ($x/l = 0.61$, Figure 4d), with flow at the bed weakly leading flow at the surface. As the flow enters the deeper zone, the reverse of flow shallowing occurs, with the magnitude of fluctuations increasing and their time (and length scales) decreasing. However, these changes are considerably less coherent than in the flow shallowing zone. This is associated with large-scale separation downstream from the region of very shallow flow (i.e., high bed elevations) such that flow recirculation effects (including eddy shedding) are superimposed upon the effects of bed resistance on flow structures. At elevations $z/h = 0.4$ and $z/h = 0.6$, the increase in magnitude of fluctuations is greater and the compression is greater. This is probably the zone of maximum influence from the eddy shedding process. The eddy shedding results in highly irregular, variable magnitude and quite complex flow. In time-averaged measurements or models, this would correspond to the zone of maximum turbulent stresses where the main flow connects with the separation zone.

[31] Figure 5 plots the correlation between downstream (u') and vertical (w') velocity deviations against distance for the complete time series down the centre line of the model simulations for four elevations above the bed. This has a notable pattern: up to $x/l = 0.21$, the strength of correlation increases with elevation above the bed. At $x/l = 0.27$, the correlations have similar values, in the range -0.28 to -0.36. Between $x/l = 0.27$ and $x/l = 0.61$, the patterns are reversed, with very strong negative correlations near the bed, and much weaker correlations higher in the flow. This pattern reverses once more at $x/l = 0.61$, with the exception of the results at $x/l = 0.70$.

3.3. Quadrant Analysis

[32] Figure 6 shows how these correlations are linked to changes in the percentage of time found in each quadrant. As expected in a turbulent boundary layer, quadrant two (ejection) and quadrant four (sweep) events are dominant. Close to the bed ($z/h = 0.2$, Figure 6a) and until $x/l = 0.27$, the distribution of events is relatively similar, with quadrant two (ejection) and four (sweep) events weakly dominant. From $x/l = 0.21$, the percentage of quadrant two (ejection) and four (sweep) events increases, with them becoming strongly dominant from $x/l = 0.46$, initially in quadrant 2 (ejection), and later in quadrant 4 (sweeps). As with the time series, there is a switch back at $x/l = 0.61$, with the exception of data at $x/l = 0.70$. This is mirrored, but to a lesser degree, at $z/h = 0.4$ (Figure 6b). Higher in the flow (at $z/h = 0.6$ and $z/h = 0.8$, Figures 6c and 6d) the percentage of events in each quadrant is, in relative terms, more constant, with quadrant two (ejection) and four (sweep) events weakly dominant throughout. Thus the correlation patterns shown in Figure 5 are related to a near-bed strengthening in the contribution of sweeps and ejections in shallowing flows: as

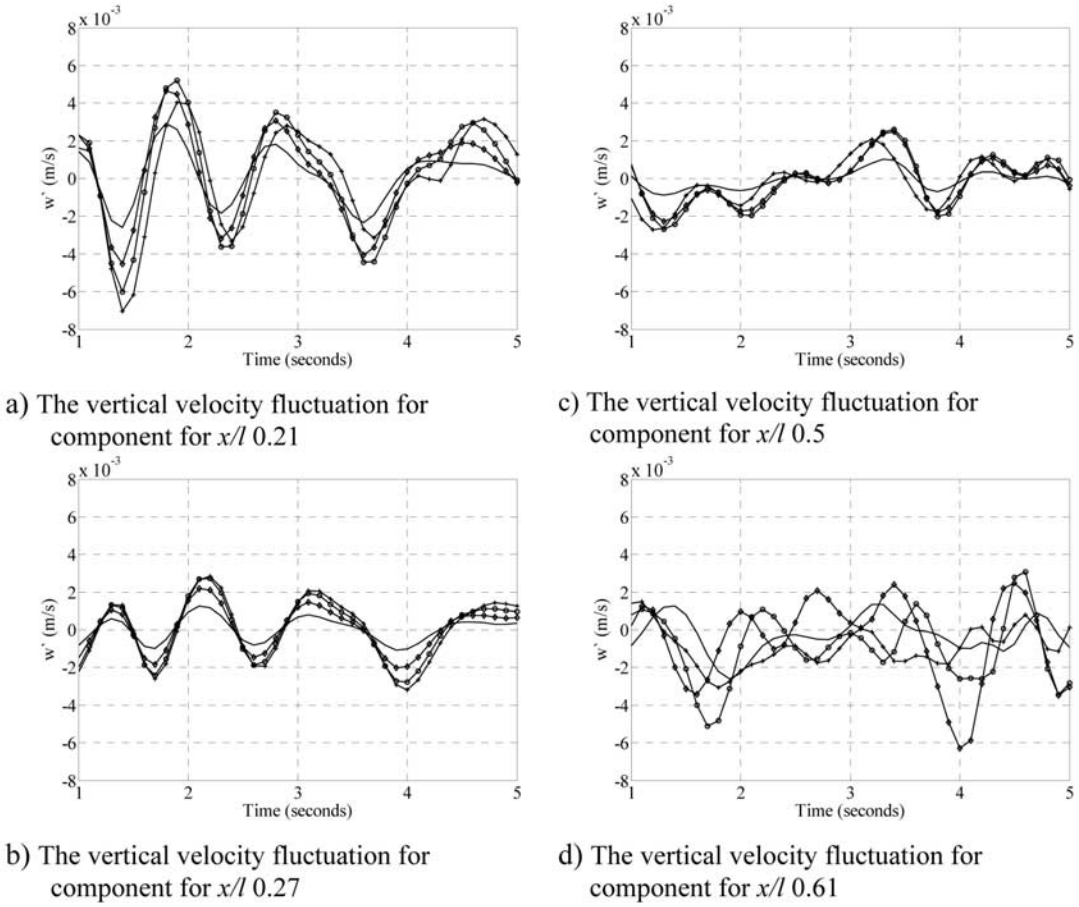

Figure 4. Time series of instantaneous vertical velocities (w') for x/l = (a) 0.21, (b) 0.27, (c) 0.50, and (d) 0.61. Pluses represent the flow at z/h = 0.2, circles represent flow at z/h = 0.4, diamonds represent flow at z/h = 0.6, and no marker indicates flow at z/h = 0.8.

the flow shallows, ejection events become dominant at the bed. Once the shallowest parts of the flow are reached, there is a transition from ejection events to sweep events becoming dominant. As the flow deepens the dominance of ejections and sweeps is reduced, except for localized points where individual clasts are found, and where ejections and sweeps are more dominant at the bed.

3.4. Spectral Analysis

[33] Finally we consider energy spectra. It has been shown that the traditional Smagorinsky model is too dissipative [*Mason and Thomson*, 1992]. In LES, the dissipation characteristics of the model have a direct impact on the turbulent kinetic energy of the resolved field, which in turn affects the shape of the mean velocity profile. There is evidence that the streamwise velocity spectra will follow a Kolmogorov $k^{-5/3}$ dependence [*Soulsby*, 1981] and deviation from this criterion may be used to identify the scale at which the scheme becomes too dissipative.

[34] The two profiles which have been identified are located at 0.21 and 0.6 x/l for the vertical heights of 0.2 and 0.8 z/h. The power spectral density graphs are shown in Figure 7. The spectral signals show classical characteristics with higher power at lower frequencies.

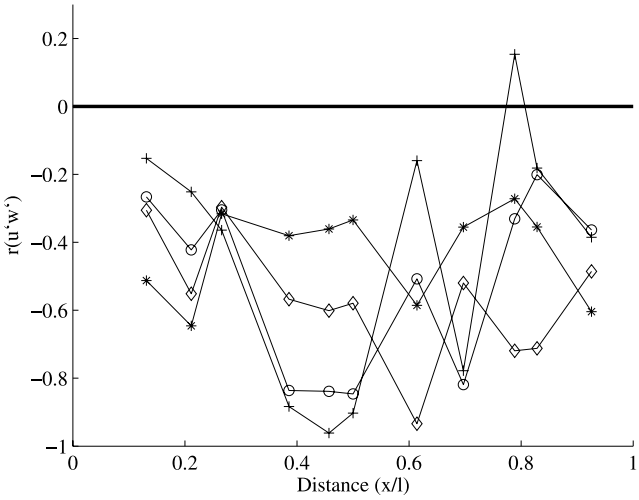

Figure 5. Correlations of the vertical and downstream instantaneous flow velocities for the whole time series. Pluses represent flow at z/h = 0.2, circles represent flow at z/h = 0.4, diamonds represent flow at z/h = 0.6, and stars represent flow at z/h = 0.8.

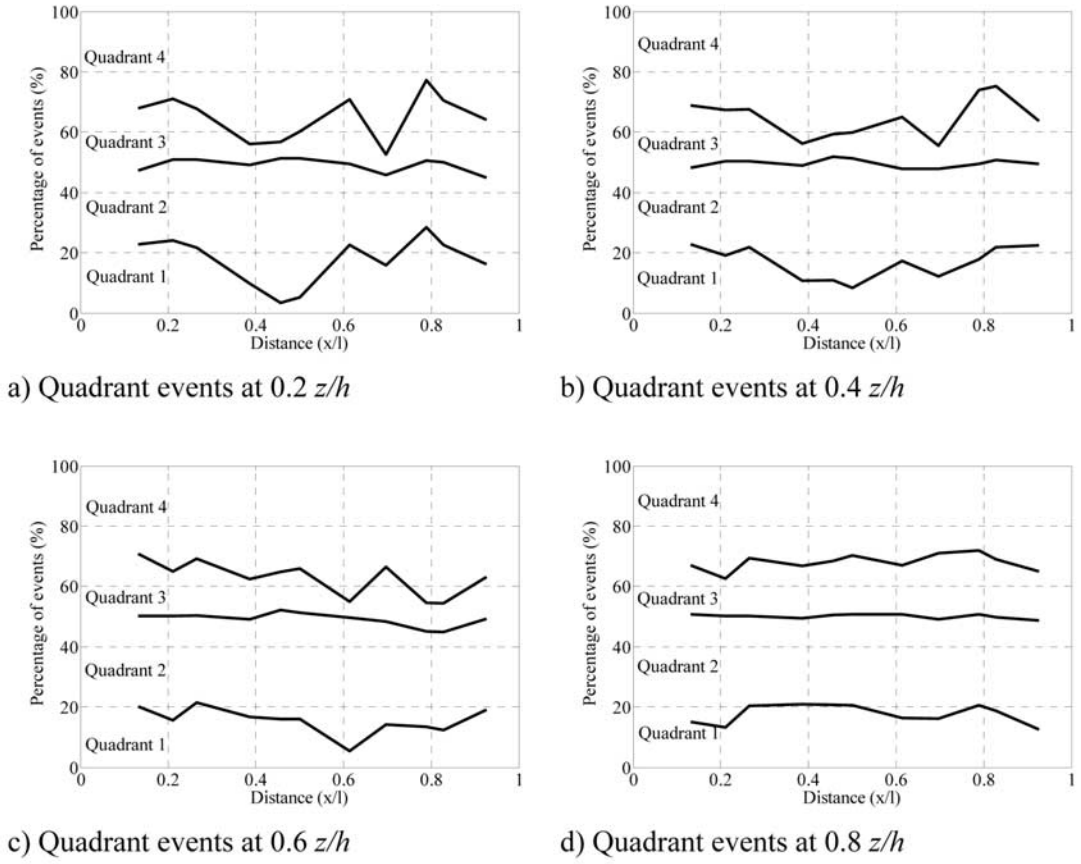

Figure 6. Cumulative percentage of events found in each quadrant downstream. (a). Quadrant events at 0.2 *z*/*h*. (b) Quadrant events at 0.4 *z*/*h*. (c) Quadrant events at 0.6 *z*/*h*. (d) Quadrant events at 0.8 *z*/*h*.

Moreover, all four profiles are similar. In assessing the performance of the Smagorinsky scheme it is clear (Figures 7a–7d) that the spectra decays significantly faster than the −5/3 gradient for frequencies greater than 2 Hz. This implies that the model dissipates kinetic energy at an excessive rate at these higher frequencies [*Porté-Agel et al.*, 2000]. The excessive dissipation of turbulent kinetic energy is greater in the shallowing zone, as would be expected, due to the shear flow as it moves over a protrusion. The standard Smaogorinsky scheme is under performing at these higher frequencies, as has been demonstrated in different environmental applications and requires improving to a scale-dependent dynamic model [*Porté-Agel et al.*, 2000]. This explains the relatively smooth nature of the time series in Figure 4 as compared with much nosier time series commonly measured in the field and laboratory studies [e.g., *Clifford and French*, 1993; *Ferguson et al.*, 1996; *Nikora and Smart*, 1997; *Roy et al.*, 1996; *Buffin-Bélanger et al.*, 2000]. However, the macroscale (<1 Hz) variability described within this study is likely to be relatively unaffected by this process showing that the longer timescale fluctuations probably do have meaning.

4. Discussion

[35] This paper has presented a methodology which enables the inclusion of complex topography within a Cartesian framework, which in turn has allowed the application of large-eddy simulation over a gravel surface. The application of LES has allowed time-dependent flow structures to be calculated interacting with a range of topographic scales from individual particles to micro topographic forms in the bed surface. Classical fluvial hydraulic structures such as arch vortices [*Hunt et al.*, 1978], in addition to regions of momentum exchange in the downstream wake of protruding clasts, have been detected and visualized which are similar to structures that have been previously measured in the field [cf. *Robert et al.*, 1993; *Kirkbride*, 1993; *Buffin-Bélanger and Roy*, 1998]. These features have previously been speculated from field-based measurements to exist in gravel bed rivers, although the hypotheses have come from several at-a-point measurements rather than studying the whole flow field as a continuum. This methodology has provided a technique for both the quantification and visualization of the complex flow structures formed by the interaction between form and flow.

[36] The numerical simulations reported in this paper have shown the importance of the localized topographic gradient on the generation of flow structures. There appears to be a difference in processes operating, and therefore the shape of the flow structures, between regions of flow shallowing and deepening. As the flow shallows, the effects of individual clasts are more strongly felt throughout the flow, where turbulent fluctuations are more synchronous

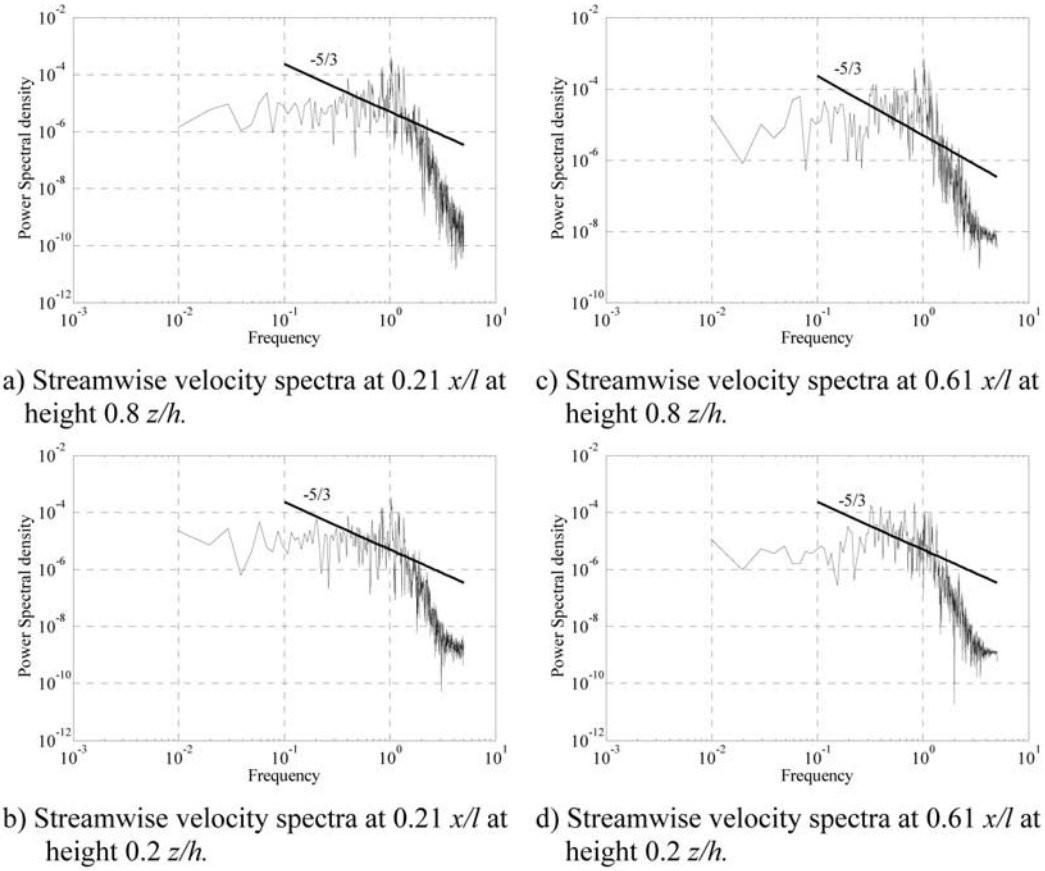

Figure 7. Streamwise velocity spectra for a shallowing region (0.21 x/l) and deepening zone (0.61 x/l). The slope of $-5/3$ is shown. (a) Streamwise velocity spectra at 0.21 x/l at height 0.8 z/h. (b) Streamwise velocity spectra at 0.21 x/l at height 0.2 z/h. (c) Streamwise velocity spectra at 0.61 x/l at height 0.8 z/h. (d) Streamwise velocity spectra at 0.61 x/l at height 0.2 z/h.

and reduced in magnitude. In addition, as the flow shallows, ejection events become dominant at the bed. These structures then evolve until they become nearly the equal to the flow depth, showing a similarity to those observed by *Yalin* [1992]. Once the shallowest part of the flow is reached, there is a transition from ejection events to sweep events becoming dominant. Finally, in shallowing zones structures are coherent as there is limited spatial scale (mainly vertical) for processes such as large-scale separation or flow recirculation (including eddy shedding) to occur and the effect of individual clasts upon flow structures is dominant, generating flow structures similar to those observed previously [cf. *Komori et al.*, 1982; *Grinvald and Nikora*, 1988; *Clifford et al.*, 1992; *Lapointe*, 1992, *Nezu and Nakagawa*, 1993; *Robert et al.*, 1993; *Roy et al.*, 1996; *Cellino and Graf*, 1999; *Shen and Lemmin*, 1999].

[37] As the flow deepens the fluctuations are more variable in terms of magnitude and timescale and, as a result, appear to be less organized. This agrees with others who do not detect any regular period in turbulent fluctuations [e.g., *Grinvald*, 1974; *Nikora and Smart*, 1997] suggesting coherent structures are randomly distributed in time and space [*Nychas et al.*, 1973; *Smith*, 1996; *Nikora and Goring*, 1999]. Moreover, as the flow deepens the dominance of ejections and sweeps is reduced, except for localized points where individual clasts are found. As the flow enters a deeper zone, there is a reverse of the processes observed in regions of flow shallowing, with the magnitude of turbulent fluctuations increasing and their time (and length scales) decreasing.

[38] In summary, there are two distinct scales of boundary influence upon the shallow flow studied here. The first, larger, scale is associated with clusters of particles which create undulations in the bed surface. This leads to water depth variation which in turn results in changes in the time and length scales and magnitudes of the associated turbulence. The second scale relates to especially large or isolated clasts which result in similar processes, but over a smaller length scale. This emphasizes that the measured flow variability at any one point in a natural river will contain both locally derived flow structures and structures inherited from upstream, according to the range of scales of topography present.

[39] The LES results give high spatial resolution in three dimensions, in a way that is currently difficult to match by laboratory measurements and impossible to match in the field using currently available technology. The methodology

is therefore seen as having considerable potential for elucidating flow structures in shallow streams and opens up exciting possibilities for exploring this effect and using it to develop new methods for parameterizing shear stress in sediment transport models. Ongoing research into this problem is addressing the SGS model where the introduction of a scale-dependent dynamic subgrid-scale model [e.g., *Porté-Agel et al.*, 2000] is being considered. This approach is both stable and robust and shows improved dissipative properties leading to more realistic spectra and mean velocity profiles being calculated [*Porté-Agel et al.*, 2000]. This approach seems to be able to resolve eddy structure more accurately, which will be advantageous to those studies that consider the detailed interaction between turbulent flows and sediment transport.

[40] **Acknowledgments.** R.J.H. was funded by NERC grant GR3/9715 (awarded to S.N.L. and R.I.F.) and NERC fellowship NER/J/S/2002/00663. We are grateful to the Associate Editor Fernando Porté-Agel and three anonymous referees for providing helpful comments that have led to significant improvements in this manuscript.

References

Bardina, J., J. H. Ferziger, and W. C. Reynolds (1980), Improved subgrid models for large eddy simulation, *AIAA J.*, *80*, 1357.

Bedford, K., and C. Babajimopoulos (1980) Verifying lake models with spectral statistics, *J. Hydraul. Div. Am. Soc. Civ. Eng.*, *106*, 21–38.

Bennett, S. J., and J. L. Best (1995), Mean flow and turbulence structure over fixed, two-dimensional dunes: implications for sediment transport and dune stability, *Sedimentology*, *42*, 491–513.

Best, J. L. (1993), On the interactions between turbulent flow, sediment transport and bedform development: Some considerations from recent experiment research, in *Turbulence: Perspectives on Flow and Sediment Transport*, edited by N. J. Clifford, J. R. French, and J. Hardisty, pp. 61–92, John Wiley, Hoboken, N. J.

Bogard, D. G., and W. G. Tiederman (1986), Burst detection with single-point velocity measurement, *J. Fluid Mech.*, *162*, 113–135.

Booker, D. J., D. A. Sear, and A. J. Payne (2001), Modelling three-dimensional flow structures and patterns of boundary shear stress in a natural pool-riffle sequence, *Earth Surf. Processes Landforms*, *26*, 553–576.

Bradbrook, K. F., S. N. Lane, K. S. Richards, P. M. Biron, and A. G. Roy (2000), Large-eddy simulation of periodic flow characteristics at river channel confluences, *J. Hydraul. Res.*, *38*, 207–215.

Bray, D. I. (1982), Flow resistance in gravel-bed rivers, in *Gravel-Bed Rivers*, edited by R. D. Hey, J. C. Bathurst, and C. R. Thorne, pp. 109–133, John Wiley, Hoboken, N. J.

Buffin-Bélanger, T., and A. G. Roy (1998), Effects of a pebble cluster on the turbulent structure of a depth-limited flow in a gravel-bed river, *Geomorphology*, *25*, 249–267.

Buffin-Bélanger, T., A. G. Roy, and A. D. Kirkbride (2000), On large scale flow structures in a gravel bed river, *Geomorphology*, *32*, 417–435.

Butler, J. B., S. N. Lane, and J. H. Chandler (1998), Assessment of DEM quality for characterising surface roughness using close range digital photogrammetry, *Photogramm. Rec.*, *16*, 271–291.

Butler, J. B., S. N. Lane, and J. H. Chandler (2001), Application of two-dimensional fractal analysis to the characterisation of gravel-bed river surface structure, *Math. Geol.*, *33*, 301–330.

Butler, J. B., S. N. Lane, J. H. Chandler, and K. Porfiri (2002), Through-water close-range digital photogrammetry in flume and field environments, *Photogramm. Rec.*, *17*, 419–439.

Cai, X.-M., and D. G. Steyn (1996), The von Karman constant determined by large eddy simulation, *Boundary Layer Meteorol.*, *78*, 143–164.

Canuto, V. M., and Y. Cheng (1997), Determination of the Smagorinsky–Lilly constant Cs, *Phys. Fluids*, *9*, 1368–1378.

Carati, D., S. Ghosal, and P. Moin (1995), On the representation of back-scatter in dynamic localization models, *Phys. Fluids*, *7*, 606–616.

Cellino, M., and W. H. Graf (1999), Sediment-laden flow in open-channels under noncapacity and capacity conditions, *J. Hydraul. Eng.*, *125*, 455–462.

Chollet, J. P., and M. Lesieur (1981), Parameterization of small scales of three-dimensional isotropic turbulence utilizing spectral closures, *J. Atmos. Sci.*, *38*, 2747–2757.

Ciofalo, M., and M. W. Collins (1992), Large-eddy simulation of turbulent flow and heat transfer in plane and rib-roughened channels, *Int. J. Numer. Methods Fluids*, *15*, 453–489.

Clark, R. A., J. H. Ferziger, and W. C. Reynolds (1979), Evaluation of subgrid models using an accurately simulated turbulent flow, *J. Fluid Mech.*, *91*, 1–16.

Clifford, N. J., and J. R. French (1993), Monitoring and analysis of turbulence in geophysical boundaries: Some analytical and conceptual issues, in *Turbulence: Perspectives on Flow and Sediment Transport*, edited by N. J. Clifford, J. R. French, and J. Hardisty, pp. 93–120, John Wiley, Hoboken, N. J.

Clifford, N. J., A. Robert, and K. S. Richards (1992), Estimation of flow resistance in gravel-bedded rivers: A physical explanation of the multiplier of roughness length, *Earth Surf. Processes Landforms*, *17*, 111–126.

Collis, S. S. (2001), Monitoring unresolved scales in multiscale turbulence modeling, *Phys. Fluids*, *13*, 1800–1806.

Cui, J., V. C. Patel, and C.-L. Lin (2003), Large-eddy simulation of turbulent flow in a channel with rib roughness, *Int. J. Heat Fluid Flow*, *24*, 372–388.

Deardorff, J. W. (1970a), A numerical study of three-dimensional turbulent channel flow at large Reynolds number, *J. Fluid Mech.*, *41*, 453–480.

Deardorff, J. W. (1970b), A three-dimensional numerical investigation of the idealized planetary boundary layer, *Geophys. Fluid Dyn.*, *1*, 377–410.

Dinehart, R. L. (1992), Evolution of coarse gravel bed forms: Field measurements at flood stage, *Water Resour. Res.*, *28*, 2667–2689.

Domaradzki, J. A., and K.-C. Loh (1999), The subgrid-scale estimation in the physical space representation, *Phys. Fluids*, *11*, 2330–2342.

Domaradzki, J. A., and E. M. Saiki (1997), A subgrid-scale model based on the estimation of unresolved scales of turbulence, *Phys. Fluids*, *9*, 2148–2164.

Falco, R. E. (1977), Coherent motions in the outer region of a turbulent boundary layers, *Phys. Fluids*, *20*, 124–132.

Ferguson, R. I., A. D. Kirkbride, and A. G. Roy (1996), Scales of turbulent coherent flow structures in gravel bedded river, in *Coherent Flow Structures in Open Channels*, edited by P. J. Ashworth et al., pp. 165–184, John Wiley, Hoboken, N. J.

Ferguson, R. I., D. R. Parsons, S. N. Lane, and R. J. Hardy (2003), Flow in meander bends with recirculation at the inner bank, *Water Resour. Res.*, *39*(11), 1322, doi:10.1029/2003WR001965.

Fröhlich, J., and W. Rodi (2002), Introduction to large eddy simulation for turbulent flows, in *Closure Strategies for Turbulent and Transitional Flows*, edited by B. E. Launder and N. D. Sandham, pp. 267–298, Cambridge Univ. Press, New York.

Germano, M. (1992), Turbulence: The filtering approach, *J. Fluid Mech.*, *238*, 325–336.

Germano, M., U. Piomelli, P. Moin, and W. H. Cabot (1991), A dynamic subgrid-scale eddy viscosity model, *Phys. Fluids A*, *3*, 1760–1765.

Gessler, D., B. Hall, M. Spasojevic, F. Holly, H. Pourtaheri, and N. Raphelt (1999), Application of 3D mobile bed, hydrodynamic model, *J. Hydraul. Eng.*, *125*, 737–749.

Geurts, B. J. (1997), Inverse modeling for large-eddy simulation, *Phys. Fluids*, *9*, 3585–3587.

Ghosal, S., T. S. Lund, P. Moin, and K. Akselvoll (1995), A dynamic localization model for large-eddy simulation of turbulent flows, *J. Fluid Mech.*, *286*, 229–255.

Grass, A. J. (1971), Structural features of turbulent flow over smooth and rough boundaries, *J. Fluid Mech.*, *50*, 233–255.

Grass, A. J., and M. Mansour-Tehrani (1996), Generalized scaling of coherent bursting structures in the near-wall region of turbulent flow over smooth and rough boundaries, in *Coherent Flow Structures in Open Channels*, edited by P. J. Ashworth et al., pp. 41–62, John Wiley, Hoboken, N. J.

Grass, A. J., R. J. Stuart, and M. Mansour-Tehrani (1991), Vortical structures and coherent motion in turbulent flow over smooth and rough boundaries, *Philos. Tran. R. Soc., Ser. A*, *336*, 35–65.

Grinvald, D. I. (1974), *Turbulence of Open-Channel Flows* (in Russian), Gidrometeoizdat, St. Petersburg, Russia.

Grinvald, D. I., and V. I. Nikora (1988), *River Turbulence* (in Russian), Gidrometeoizdat, St. Petersburg, Russia.

Grishanin, K. V. (1990), *Fundamentals of the Dynamics of Alluvial Flows* (in Russian), Transport, Moscow.

Gullbrand, J., and F. K. Chow (2003), The effect of numerical errors and turbulence models in large-eddy simulation of channel flow, with and without explicit filtering, *J. Fluid Mech.*, *495*, 323–341.

Hardy, R. J., S. N. Lane, M. R. Lawless, J. L. Best, L. Elliott, and D. B Ingham (2005), Development and testing of a numerical code for treatment of complex river channel topography in three-dimensional CFD models with structured grids, *J. Hydraul. Res.*, *43*, 468–480.

Härtel, C. (1996), Turbulent flows: Direct numerical simulation and large-eddy simulation, in *Handbook of Computational Fluid Mechanics*, edited by R. Peyret, pp. 283–338, Elsevier, New York.

Härtel, C., and L. Kleiser (1997), Galilean invariance and filtering dependence of near-wall grid-scale/subgrid-scale interactions in large-eddy simulation, *Phys. Fluids A*, *9*, 473–475.

Härtel, C., and L. Kleiser (1998), Analysis and modelling of subgridscale motions in near-wall turbulence, *J. Fluid Mech.*, *356*, 327–352.

Head, M. R., and P. Bandyopadhyay (1981), New aspects of turbulent boundary layer structure, *J. Fluid Mech.*, *107*, 297–338.

Hey, R. D. (1979), Flow resistance in gravel-bed rivers, *J. Hydraul. Div. Am. Soc. Civ. Eng.*, *105*, 365–379.

Hodskinson, A., and R. I. Ferguson (1998), Numerical modelling of separated flow in river bends: Model testing and experimental investigation of geometric controls on the extent of flow separation at the concave bank, *Hydrol. Processes*, *12*, 1323–1338.

Hughes, T. J. R., G. R. Feijoo, L. Mazzei, and J. B. Quincy (1998), The variational multiscale method—A paradigm for computational mechanics, *Comput. Methods Appl. Mech.*, *166*, 3–4.

Hughes, T. J. R., L. Mazzei, A. A. Oberai, and A. A. Wray (2001a), The multiscale formulation of large eddy simulation: Decay of homogeneous isotropic turbulence, *Phys. Fluids*, *13*, 505–512.

Hughes, T. J. R., A. A. Oberai, and L. Mazzei (2001b), Large eddy simulations of turbulent channel flow by the variational multiscale method, *Phys. Fluids*, *13*, 1784–1799.

Hunt, J. C. R., C. J. Abell, J. A. Peterka, and H. Woo (1978), Kinematic studies of the flow around free or surface mounted obstacles: Applying topology to flow visualization, *J. Fluid Mech.*, *86*, 179–200.

Imamoto, H., and T. Ishigaki (1986a), The three dimensional structure of turbulent shear flow in an open channel, paper presented at Fifth Congress of the Asian and Pacific Regional Division of the International Association for Hydraulic Research, Seoul.

Imamoto, H., and T. Ishigaki (1986b), Visualization of longitudinal eddies in an open channel flow, in *Flow Visualization IV: Proceedings of the Fourth International Symposium on Flow Visualization*, edited by C. Veret, pp. 333–337, Taylor and Francis, Philadelphia, Pa.

Keylock, C. J., R. J. Hardy, D. R. Parsons, R. I. Ferguson, S. N. Lane, and K. S. Richards (2005), The theoretical foundations and potential for large-eddy simulation (LES) in fluvial geomorphic and sedimentological research, *Earth Sci. Rev.*, *71*, 271–304.

Kirkbride, A. D. (1993), Observations of the influence of bed roughness on turbulence structure in depth-limited flows over gravel beds, in *Turbulence: Perspectives on Flow and Sediment Transport*, edited by N. J. Clifford, J. R. French, and J. Hardisty, pp. 185–196, John Wiley, Hoboken, N. J.

Kirkbride, A. D., and R. I. Ferguson (1995), Turbulent flow structures in a gravel-bed river: Markov chain analysis of the fluctuating velocity profile, *Earth Surf. Processes Landforms*, *20*, 721–733.

Klaven, A. B. (1966), Investigation of the flow turbulent structure (in Russian), *Trans. State Hydrol. Inst.*, *136*, 65–76.

Klaven, A. B., and Z. D. Kopaliani (1973), Laboratory investigations of the kinematic structure of turbulent flow over a rough bed (in Russian), *Trans. State Hydrol. Inst.*, *209*, 67–90.

Komori, S., H. Ueda, F. Ogino, and T. Mizushina (1982), Turbulence structure and transport mechanism at the free surface in an open channel flow, *Int. J. Heat Mass Transfer*, *25*, 513–521.

Krogstad, P. Å., R. A. Antonia, and W. B. Browne (1992), Comparison between rough and smooth-wall turbulent boundary layers, *J. Fluid Mech.*, *245*, 599–617.

Lane, S. N., R. J. Hardy, L. Elliott, and D. B. Ingham (2002), High resolution numerical modelling of three-dimensional flows over complex river bed topography, *Hydrol. Processes*, *16*, 2261–2272.

Lane, S. N., R. J. Hardy, L. Elliott, and D. B. Ingham (2004), Numerical modelling of flow processes over gravelly surfaces using structured grids and a numerical porosity treatment, *Water Resour. Res.*, *40*, W01302, doi:10.1029/2002WR001934.

Lapointe, M. (1992), Burst-like sediment suspension events in a sand bed river, *Earth Surf. Processes Landforms*, *17*, 253–270.

Lee, C. (2002), Large-eddy simulation of rough wall turbulent boundary layers, *AIAA J.*, *40*, 2127–2130.

Leonard, A. (1974), Energy cascade in large-eddy simulations of turbulent fluid flows, *Adv. Geophys., Ser. A*, *18*, 237–248.

Lesieur, M., and O. Métais (1996), New trends in large-eddy simulations of turbulence, *Annu. Rev. Fluid Mech.*, *28*, 45–82.

Lesieur, M., P. Comte, E. Lamballais, O. Métais, and G. Silvestrini (1997), Large-eddy simulations of shear flows, *J. Eng. Math.*, *32*, 195–215.

Lesieur, M., P. Comte, Y. Dubief, E. Lamballais, O. Métais, and S. Ossia (1999), From two-point closures of isotropic turbulence to LES of shear flows, *Flow Turbul. Combust.*, *63*, 247–267.

Lilly, D. K. (1992), A proposed modification of the Germano subgrid-scale closure method, *Phys. Fluids A*, *4*, 633–635.

Lu, S. S., and W. W. Willmart (1973), Measurements of structure of Reynolds stress in a turbulent boundary layer, *J. Fluid Mech.*, *60*, 481–511.

Mason, P. J., and D. Thomson (1992), Stochastic backscatter in large eddy simulations of boundary layers, *J. Fluid Mech.*, *242*, 51–78.

Meneveau, C., and J. Katz (1999), Dynamic testing of subgrid models in large eddy simulation based on the Germano identity, *Phys. Fluids*, *11*, 245–247.

Meneveau, C., and J. Katz (2000), Scale-invariance and turbulence models for large-eddy simulation, *Annu. Rev. Fluid Mech.*, *32*, 1–32.

Meneveau, C., T. S. Lund, and W. H. Cabot (1996), A Lagrangian dynamic subgrid-scale model of turbulence, *J. Fluid Mech.*, *319*, 353–385.

Moin, P. (2002), Advances in large eddy simulation methodology for complex flows, *Int. J. Heat Fluid Flow*, *23*, 710–720.

Moin, P., and J. Kim (1982), Numerical investigation of turbulent channel flow, *J. Fluid Mech.*, *118*, 341–377.

Moin, P., K. Squires, W. Cabot, and S. Lee (1991), A dynamic subgridscale model for compressible turbulence and scalar transport, *Phys. Fluids A*, *3*, 1766–1771.

Nezu, I., and H. Nakagawa (1993), *Turbulence in Open Channel Flows*, A. A. Balkema, Brookfield, Vt.

Nicholas, A. P. (2001), Computational fluid-dynamics modelling of boundary roughness in gravel-bed rivers: An investigation of the effects of random variability in bed elevation, *Earth Surf. Processes Landforms*, *26*, 345–362.

Nicholas, A. P., and G. H. S. Smith (1999), Numerical simulation of three-dimensional flow hydraulics in a braided channel, *Hydrol. Processes*, *13*, 913–929.

Nikora, V. I., and G. Goring (1999), On the relationship between Kolmogorov's and generalized structure functions in the inertial subrange of developed turbulence, *J. Phys. A Math. Gen.*, *32*, 4963–4969.

Nikora, V. I., and G. M. Smart (1997), Turbulence characteristics of New Zealand gravel-bed rivers, *J. Hydraul. Eng.*, *123*, 764–773.

Nychas, S. G., H. C. Hershey, and R. S. Brodkey (1973), A visual study of turbulent shear flow, *J. Fluid Mech.*, *61*, 513–540.

Olsen, N. R. B., and S. Stokseth (1995), Three-dimensional numerical modelling of water flow in a river with large bed roughness, *J. Hydraul. Res.*, *33*, 571–581.

Patankar, S. V., and D. B. Spalding (1972), A calculation procedure for heat, mass and momentum transport in three-dimensional parabolic flows, *Int. J. Heat Mass Transfer*, *15*, 1787–1806.

Patel, V. C. (1998), Perspective: Flow at high Reynolds number and over rough surfaces—Achilles heel of CFD, *J. Fluids Eng.*, *120*, 434–444.

Piomelli, U., and E. Balaras (2000), Wall-layer models for large-eddy simulations, *Annu. Rev. Fluid Mech.*, *34*, 349–374.

Piomelli, U., and J. Liu (1995), Large-eddy simulation of rotating channel flows using a localized dynamic model, *Phys. Fluids*, *7*, 839–848.

Piomelli, U., T. A. Zang, C. G. Speziale, and M. Y. Hussaini (1990), On the large-eddy simulation of transitional wall bounded flows, *Phys. Fluids A*, *2*, 257–265.

Porté-Agel, F., C. Menevveau, and M. B. Parlange (2000), A scale-dependent dynamic model for large-eddy simulation: Application to a neutral atmospheric boundary layer, *J. Fluid Mech.*, *415*, 261–284.

Robert, A., A. G. Roy, and B. De Serres (1993), Space-time correlations of velocity measurements at a roughness transition in a gravel-bed river, in *Turbulence: Perspectives on Flow and Sediment Transport*, edited by N. J. Clifford, J. R. French, and J. Hardisty, pp. 165–184, John Wiley, Hoboken, N. J.

Rodi, W., J. H. Ferziger, M. Breuer, and M. Pourquie (1997), Status of large eddy simulation: Results of a workshop, *J. Fluids Eng.*, *119*, 248–262.

Rogallo, R. S., and P. Moin (1984), Numerical simulation of turbulent flows, *Annu. Rev. Fluid Mech.*, *16*, 99–137.

Roy, A. G., and T. Buffin-Belanger (2000), Advances in the study of turbulent flow structures in gravel-bed rivers, in *Gravel-Bed Rivers V*, edited by M. P. Mosley, pp. 375–404, N. Z. Hydrol. Soc., Wellington.

Roy, A. G., T. Buffin-Belanger, and S. Deland (1996), Scales of turbulent coherent structures in a gravel-bed river, in *Coherent Flow Structures in Open Channels*, edited by P. J. Ashworth et al., pp. 147–156, John Wiley, Hoboken, N. J.

Roy, A. G., T. Buffin-Belanger, H. Lamarre, and A. D. Kirkbride (2004), Size, shape and dynamics of large-scale turbulent flow structures in a gravel-bed river, *J. Fluid Mech.*, *500*, 1–27.

Sagaut, P. (1998), *Large Eddy Simulation for Incompressible Flows*, Springer, New York.

Schumann, U. (1975), Subgrid scale model for finite difference simulations of turbulent flows in plane channels and annuli, *J. Comput. Phys.*, *18*, 376–404.

Schumann, U. (1991), Direct and large eddy simulation of turbulence—Summary of the state-of-the-art 1991, in *Introduction to the Modeling of Turbulence*, Von Karman Inst., Rhode Saint Genèse, Brussels.

Sechet, P., and B. Le Guennec (1999), Bursting phenomenon and incipient motion of solid particles in bed-load transport, *J. Hydraul. Res.*, *37*, 683–696.

Shen, C., and U. Lemmin (1999), Application of an acoustic particle flux profiler in particle-laden open-channel flow, *J. Hydraul. Res.*, *37*, 407–419.

Shvidchenko, A., and G. Pender (2001), Macroturbulent structure of open-channel flow over gravely beds, *Water Resour. Res.*, *37*, 709–719.

Silveira Neto, A., D. Grand, O. Métais, and M. Lesieur (1991), Large eddy simulation of the turbulent flow in the downstream region of a backward-facing step, *Phys. Rev. Lett.*, *66*, 2320–2323.

Sinha, S. K., F. Sotiropoulos, and A. J. Odgaard (1998), Three-dimensional numerical model for flow through natural rivers, *J. Hydraul. Eng.*, *124*, 13–24.

Smagorinsky, J. (1963), General circulation experiments with the primitive equations. Part I: The basic experiment, *Mon. Weather Rev.*, *91*, 99–167.

Smith, C. R. (1996), Coherent flow structures in smooth-wall turbulent boundary layers: Facts, mechanisms and speculation, in *Coherent Flow Structures in Open Channels*, edited by P. J. Ashworth et al., pp. 1–40, John Wiley, Hoboken, N. J.

Smith, C. R., J. D. A. Walker, A. H. Haidari, and U. Sobrun (1991), On the dynamics of near-wall turbulence, *Philos. Trans. R. Soc. London, Ser. A*, *336*, 131–175.

Soulsby, R. L. (1981), Selecting record length and digitization rate for near bed turbulence measurements, *J. Phys. Oceanogr.*, *10*, 208–219.

Stolz, S., and N. A. Adams (1999), An approximate deconvolution procedure for large-eddy simulation, *Phys. Fluids*, *11*, 1699–1701.

Stolz, S., N. A. Adams, and L. Kleiser (2001), An approximate deconvolution model for large eddy simulation with application to incompressible wall-bounded flows, *Phys. Fluids*, *13*, 997–1015.

Sumer, B. M., and R. Deigaard (1981), Particle motions near the bottom in turbulent flow in an open channel, part 2, *J. Fluid Mech.*, *109*, 311–337.

Talmon, A. M., J. M. G. Kunen, and G. Oooms (1986), Simultaneous flow visualisation and Reynolds stress measurement in a turbulent boundary layer, *J. Fluid Mech.*, *63*, 459–478.

Vreman, B., B. Geurts, and H. Kuerten (1994), Realizability conditions for the turbulent stress tensor in large eddy simulation, *J. Fluid Mech.*, *278*, 351–362.

Whiting, P. J., and W. E. Dietrich (1990), Boundary shear stress and roughness of mobile alluvial beds, *J. Hydraul. Eng.*, *116*, 1495–1511.

Wiberg, P. L., and J. D. Smith (1991), Velocity distribution and bed roughness in high gradient streams, *Water Resour. Res.*, *27*, 825–838.

Yalin, M. S. (1992), *River Mechanics*, 219 pp., Elsevier, New York.

Zang, Y., R. L. Street, and J. R. Koseff (1993), A dynamic mixed subgrid-scale model and its application to turbulent recirculating flows, *Phys. Fluids A*, *5*, 3186–3196.

Zedler, E. A., and R. L. Street (2001), Large-eddy simulation of sediment transport: Currents over ripples, *J. Hydraul. Eng.*, *127*, 444–452.

R. I. Ferguson, R. J. Hardy, and S. N. Lane, Department of Geography, University of Durham, Science Site, South Road, Durham DH1 3LE, UK. (r.j.hardy@durham.ac.uk)

D. R. Parsons, School of Earth and Environment, University of Leeds, Woodhouse Lane, Leeds LS2 9JT, UK.